Dynamics of Photogenerated Surface Charge on $BiFeO_3$ Films

Feng Yan,[†,‡] Guannan Chen,[†] Li Lu,[‡] and Jonathan E. Spanier[†,*]

[†]Department of Materials Science & Engineering, Drexel University, Philadelphia, Pennsylvania 19104, United States and [‡]Department of Mechanical Engineering, National University of Singapore, Singapore 117576

ABSTRACT We report on the spatial and temporal evolution of photoinduced charge generation and carrier separation in heteroepitaxial $BiFeO_3$ thin films deposited on Nb:$SrTiO_3$ as measured in ambient at room temperature with Kelvin probe and piezoresponse force microscopy. Contributions from the self-poled and ferroelectric polarization charge are identified from the time evolution of the correlated surface potential and ferroelectric polarization in films as grown and following poling, and at different stages and intensities of optical illumination. Variations in the surface potential with bias voltage, switching history, and illumination intensity indicate how both bulk ferroelectric photovoltaic and the domain wall offset potential mechanisms contribute to the photogenerated charge.

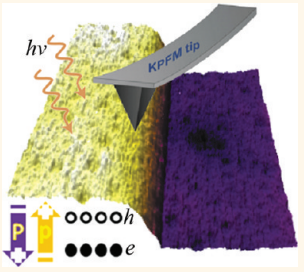

KEYWORDS: ferroelectric photovoltaics · $BiFeO_3$ · Kelvin probe microscopy

Ferroelectric semiconductors are attractive candidate photovoltaics for replacement of conventional silicon-based bipolar junctions owing to efficient ferroelectric polarization-driven carrier separation.[1−3] Much attention has been focused on the bulk photovoltaic effect in traditional ferroelectric materials[4] such as $BaTiO_3$ and $Pb(Zr,Ti)O_3$, which possess band gaps in the ultraviolet,[5] and on the local photoinduced charge dynamics on the surfaces of $BaTiO_3$.[6] Among ferroelectric oxide perovskites, $BiFeO_3$ (BFO) is distinguished by having a band gap in the visible (*ca.* 2.6−2.8 eV[3,7]) and possessing room-temperature intrinsic multiferroic properties permitting several modes of investigating and controlling the photovoltaic effect. The photovoltaic effect in BFO has both bulk and domain wall contributions: the former is due to ferroelectric polarization[5] and the latter also involves ferroelastic domains.[2] Potential offsets owing to the presence of domain walls enable a more efficient separation of carriers, and a net potential difference evolves across the entire sample.[2] Alexe *et al.*,[3] using a scanned local probe to collect the enhanced photogenerated carriers, reported that the anomalous photoexcited carriers in a BFO single crystal exist over the entire crystal and do not recombine within the ferroelastic domains.

The understanding of issues relating to the dynamic processes of charge generation and transport in BFO remains limited, however. Collection and analysis of the evolution of the surface potential (SP) owing to the photoinduced charge permit study of the effects of polarization on exciton transport and quantitative analysis of the effect of domain wall number. Kelvin probe force microscopy (KPFM)[8−13] remains a powerful noncontact local probe of SP, including SP arising from photoexcited charge.[8] Here we report on the use of KPFM, in conjunction with piezoresponse force microscopy (PFM), to probe the local spatiotemporal evolution of the SP in BFO at different stages of illumination and switching arising from the separation of carriers. We describe quantitatively both the influences of the orientation of ferroelectric polarization and of the domain wall on the measured SP of the BFO film associated with piezoresponse force microscopy (PFM). A direct visualization of charge generation and recombination enables further insight into the roles of ferroelectric polarization and domain walls on charge transfer and diffusion in BFO.

RESULTS AND DISCUSSION

Following the writing of a small square pattern with $V_{tip} = -9.8$ V within a larger square pattern ($V_{tip} = +9.8$ V, contrast in the SP (Figure 1a), the plane-normal component of piezoelectric displacement amplitude (Figure 1b) obtained sequentially in the dark can be discerned. The as deposited, unpoled area of the film exhibits a preferential outward film-normal component of polarization (as seen in the perimeter of the scan area that appears orange on the color

* Address correspondence to spanier@drexel.edu.

Received for review November 21, 2011 and accepted February 7, 2012.

Published online February 07, 2012
10.1021/nn204604m

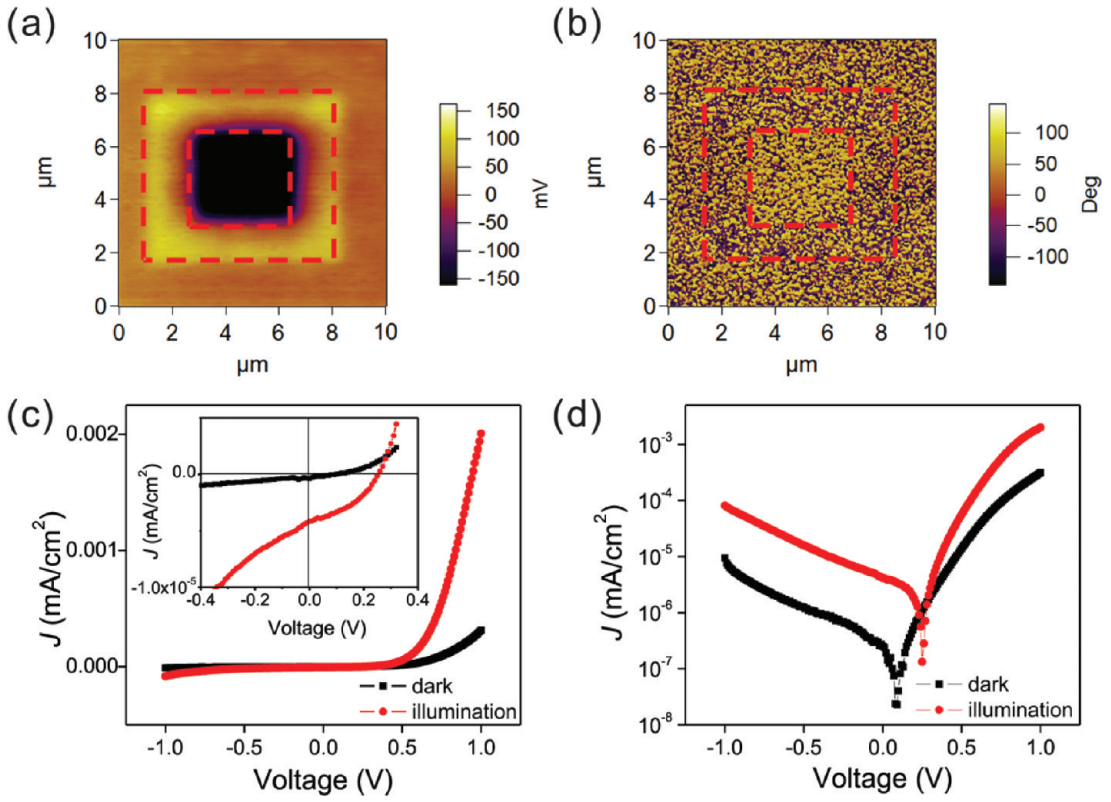

Figure 1. (a) KPFM image collected using a scan rate of 0.3 Hz following application of dc voltages of +9.8 V (while scanning at 1.0 Hz within the larger box denoted by the red dashed lines) and −9.8 V (applied while scanning within the smaller interior box, also at 1.0 Hz), and (b) corresponding film plane-normal PFM image for image a, also collected at 0.3 Hz. (c) *J*−*V* curve of a BFO/NSTO structure in the dark and under illumination. The inset shows an expanded view of *J*−*V* curves near zero bias voltage. (d) *J*−*V* curves plotted on a semilog scale.

map) due to self-poling caused by the electric field that arises due to the interfacial potential barrier between the BFO and NSTO. The large SP differences between (i) the outer and inner regions of poling as seen by the yellow and black areas in Figure 1a and (ii) each in relation to the surrounding unpoled area are due to the induced ferroelectric polarization charges and screened charges under given biases, respectively. The SP contrast (Figure 1a) is much stronger than that in the PFM image (Figure 1b), and suggests complementarity of KPFM in analyzing photogenerated charges. Macroscopically, these films exhibit a significant photovoltaic response and nonzero short-circuit current density (J_{sc} = -4.5×10^{-6} mA/cm^2 and an open circuit voltage V_{oc} of 0.26 V under an illumination intensity of ~10 mW/cm^2) owing to the self-polarization of BFO[5] (Figure 1c). The photovoltaic efficiency amounts to $\sim 1.2 \times 10^{-5}$%, much smaller than other reported values for BFO[14] because of the low transmissivity of the Pt top electrode. The data in Figure 1d are plotted on a semilog scale where the change in conductivity upon illumination is the result of excitation across a BFO/NSTO *p*−*n* junction,[15] in addition to the strong rectifying character.

Since KPFM can be taken as a measure of the electrostatic interactions between the conductive tip and sample, contributions to the obtained SP from the BFO and NSTO can be analyzed as parallel capacitances.[11,16,17] Schematic interfacial band diagrams are sketched (Figure 2), where the BFO film and NSTO substrate are assumed to be nondegenerate semiconductors[15] and the Fermi level of NSTO is in the vicinity of the bottom of the conduction band. A Schottky-like barrier is at the tip−sample interface which is modified by the local ferroelectric polarization,[18,19] and the polarization causes the conduction and valence bands to bend at the interface and produce surface charge with opposite sign on the different domain at low bias[19] (Figure 2a). When tip is brought in contact with the sample (in the absence of Fermi level pinning) Fermi level alignment takes place (Figure 2b), inducing an electrostatic force that depends on the SP difference (SP_1).[8] In the KPFM measurement, an external voltage V_{dc1} is applied to the probe in order to nullify SP_1 (flatband case, Figure 2c). To relate the KPFM measurement to the photovoltaic effect of BFO, we sketch a band diagram under illumination for the as deposited film (Figure 2d), where a photon is incident upon the top surface of BFO and an exciton is separated, producing a gradient in the quasi-Fermi levels.[20] Here, a surface photovoltage (V_{ph}) produces a surface photopotential (SP_{ph}).

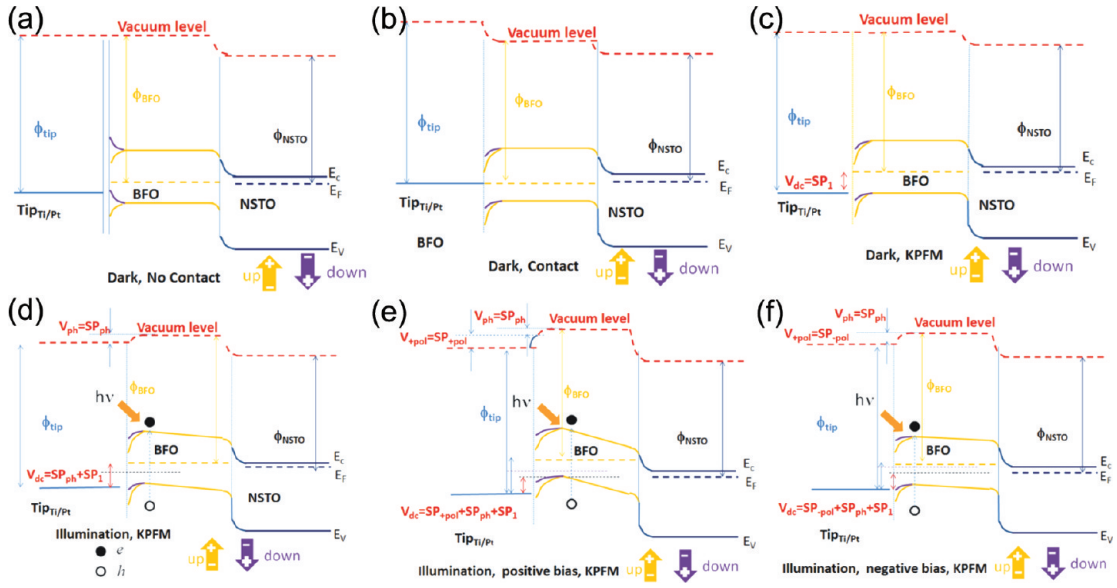

Figure 2. Idealized schematic band diagrams of interfacial band diagram Pt tip/BFO interface and BFO/NSTO heterojunction. Φ is the work function of metal and oxide; E_C, E_V, and E_F denote, respectively, the conduction band, valence band, and Fermi level of oxide. V_{dc}, SP_1, SP_{ph}, SP_{+pol}, and SP_{-pol} denote the applied dc bias for KPFM measurement, surface potential for vacuum level alignment, surface potential under illumination, surface potential under positive bias, and surface potential under negative bias, respectively. The band diagrams shown are (a) before contact among tip (Pt), sample (BFO), and substrate (NSTO) where the local ferroelectric polarization bends between tip and sample interface as illustrated; (b) electrical contact in dark; (c) flatband when applied $V_{dc} = SP_1$, the two vacuum level align between tip and BFO, nullifying the work function difference; (d) under illumination with no bias; (e) under illumination with positive bias; and (f) under illumination with negative bias.

To study the influence of polarization orientation on the response, we focus on the ferroelectric polarization-induced SP under illumination. When a positive bias voltage is applied, a net forward electron current is formed with the nullified $V_{dc} = V_{+pol}$ (Figure 2e). When a negative bias is applied under illumination, the needed V_{dc} to satisfy the nulling condition is V_{-pol} (Figure 2f). Thus, observation of SP differences can be used to discern separation of photogenerated excitons and the effect of polarization on the charge transfer in BFO. The measured change in SP can be written as $\Delta SP = \phi_{tip} - (\phi_{BFO} + \Phi_{ph} + \Phi_{FE})$, where ϕ_{tip} is the tip work function (=5.6 eV), ϕ_{BFO} is the work function of BFO (=4.7 eV),[15] Φ_{ph} is the barrier from photovoltaic effect, and Φ_{FE} is the barrier from the ferroelectric polarization.

The effect of illumination intensity on photoinduced SP was measured: distributions of SP as measured within a $5 \times 5\ \mu m^2$ area in dark and under selected values of illumination intensity are shown in Figure 3a. The distribution of SP under dark is shifted toward lower SP with respect to the cases of illumination, indicating the presence of excess photogenerated holes on the surface under continuous illumination. With increased illumination intensity, the shift in mean SP (and line width of the distribution) is seen to be saturated in the range of intensities around 158 and 166 mW/cm^2 for the values of incident intensity we used (the V_{oc} remains constant in this range). The modified SP due to the photovoltaic effect is readily observable *via* mapping the SP over this area under dark (for the first half of the scan) and then under illumination (Figure 3b). A representative section of the SP extracted from Figure 3b is presented in Figure 3c where the SP increases when the BFO is illuminated with $\Delta SP \approx 0.16$ V, with an exponential-like onset of larger SP. These positive shifts from dark to light arise from charge separation of the photogenerated electron−hole pairs with s drifting of holes to the surface and electrons to the NSTO substrate under the self-poled polarization-induced internal electric field, owing to the bulk photovoltaic effect.

To quantify the observed dynamic charging, measurements of the time-dependent SP evolution were performed. The sample was illuminated at the saturation power (158 mW/cm^2) and the time evolution of SP was measured at different locations on the sample surface. The average SP is seen to vary as the light is switched on and off (Figure 3d). During an on/off cycle, the SP saturates more quickly in the off/on transition as compared to the characteristic decay time scale in the on/off transition, corresponding to the charging and discharging processes. Both measured SP changes trend according to a single exponential, that is, $SP(t) = SP_{d,l}e^{-t/\tau_{d-l,l-d}}$ where $SP_{d,l}$ are the initial values, and $\tau_{d-l,l-d}$ are mean onset and decay lifetimes for dark-to-light and light-to-dark). Estimated lifetimes for charging and discharging (~7.6 and ~31.5 s, respectively) indicate that while the surface retains charge on the time scale of seconds, the discharging time appears to be longer than for charging and may be explained by the release of electrons from shallow

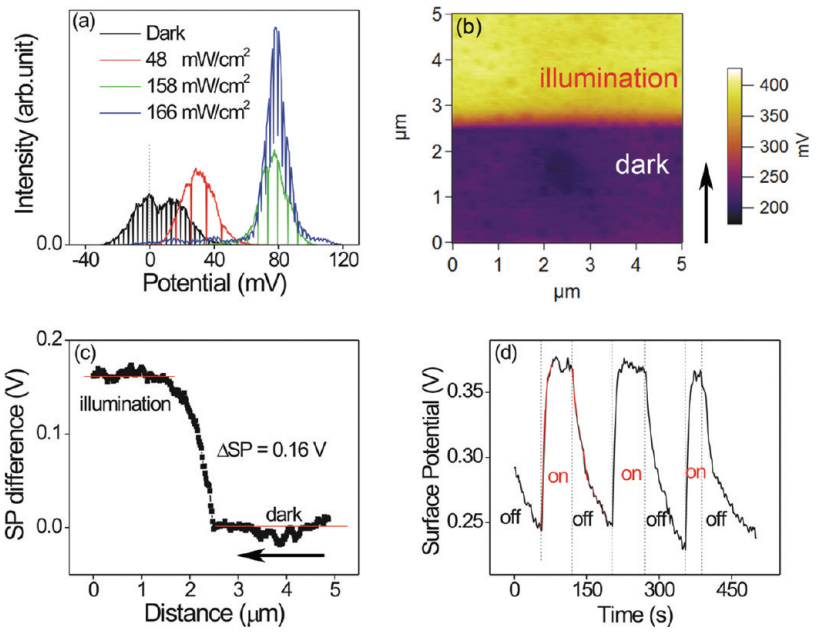

Figure 3. (a) Distributions of surface potential values as collected from a single 5 × 5 μm^2 area of the BFO/NSTO heterojunction in the dark and under illumination (48, 158, and 166 mW/cm^2). (b) KPFM image in the dark (bottom portion of scan) and under illumination (top), 158 mW/cm^2. (c) Corresponding SP profile of panel b; the arrows in panels b and c denote the slow scan axis, and scan progression, respectvely. (d) Time evolution of the surface potential of BFO turning on and off the illumination (158 mW/cm^2), indicative of exponential charging and discharging processes.

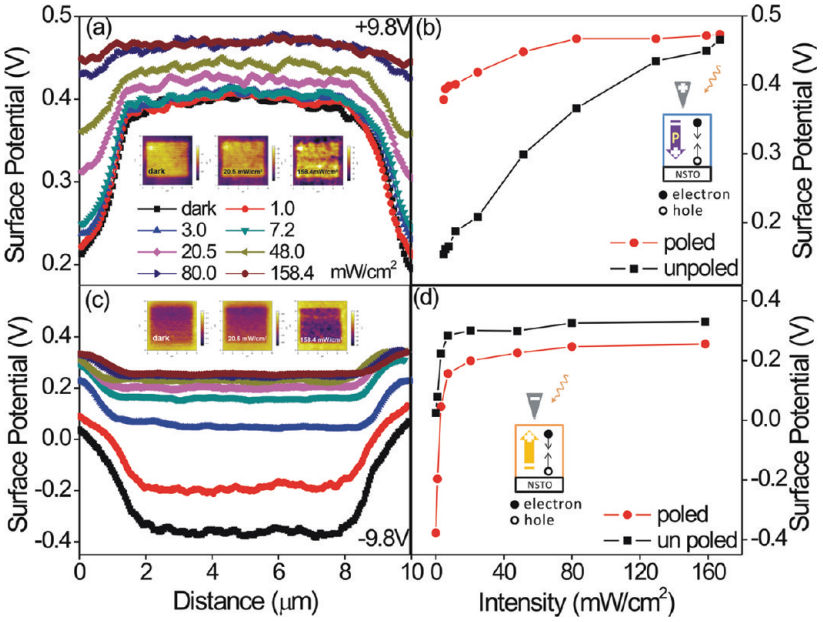

Figure 4. (a,c) Demonstration of the effect of direction of polarization on SP profile under $V_{tip} = \pm 9.8$ V. The inset images are KPFM images under different illumination intensities. (b and d), corresponding poled and unpoled area surface potential as a function of light intensity from panels a and c, respectively. The insets of panels b and d illustrate the photogeneration processes under different polarization orientation.

traps[9] (*i.e.*, oxygen vacancies[21]), or electrostatic potential offset across the domain walls of BFO film.[2,4] (This asymptotic charging and discharging behavior is obviously orders of magnitude slower than the photoexcited charge generation and recombination.) The full width at half-maximum (fwhm) is seen to decrease with increasing illumination intensity and is accompanied by a saturation of the fwhm at higher intensity. We propose that the narrowing of the line width can be accounted for by polar asymmetry in the surface charge dynamics: it is straightforward to show that the observed reduction in standard deviation of the SP distribution for increasing illumination intensity is consistent with a recombination of photoinduced

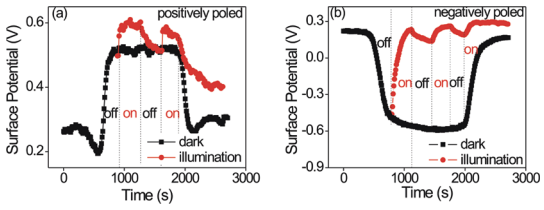

Figure 5. Time evolution of the surface potential under (a) positive and (b) negative poling of BFO under alternating dark and illumination (158 mW/cm^2) conditions.

negative charge on a faster time scale than positive charge.

It is well-known that the photovoltaic response in a ferroelectric can be controlled by electric field as a result of the reversed domain switching.[1,2,5] To understand the effect of direction of polarization on the observed photoinduced charges, the SP was measured prior to and following reorientation of polarization. Shown in Figure 4a,c are the spatial profiles of SP for the poled area for downward and upward polarization under different selected values of illumination intensity, respectively. As expected, the poled area exhibits a different SP behavior compared with the as-deposited (unpoled) portions. Meanwhile, the diode-forward direction is the same as the polarization under an external electric field.[1,2] For the poled area under illumination, the observed SP arises from (i) charges injected from the conductive tip, from (ii) screened polarization charges of the oriented dipoles, and from (iii) the photoinduced charges. In addition, the SP is observed to increase with an increase in the illumination intensity, as shown in Figure 4 panels b and d for the as-grown (unpoled), positively and negatively poled films, respectively, in accordance with the photovoltaic effect. With increasing illumination intensity, the SP of the negatively poled area saturates with lower illumination intensity, while the positively poled area requires higher illumination intensity to reach saturation. These observations indicate that the photoinduced electron−hole pairs are separated and recombine with the injected charges from the tip. Under positive bias (here, polarization is downward, as shown in the inset of Figure 4b), the injected and photoinduced holes are compensated by the produced negative polarization charges, thus the SP increases slowly as a function of intensity. Under negative bias (here, polarization is upward, as shown in the inset of Figure 4d), the photoinduced holes and produced positive polarization charges recombined with the injected negative charges (*i.e.*, electrons) at the surface and led to the sharp increase and saturation of SP (Figure 4d).

To quantify the effects of polarization direction on the evolution of surface charge density, time dependencies of the SP of the poled area in the dark and under illumination were also measured (Figure 5). For the positively poled area (Figure 5a) the SP increased sharply in the poled area when the illumination is turned on. However, removing the illumination caused the SP to relax more slowly, with average lifetimes for charging and discharging of 19.5 and 144.4 s, respectively. Our observation of a longer lifetime for the poled area as compared with that for the unpoled area (Figure 5a) suggests that a further increase of surface potential could be limited because of the suppression or delay of charge migration into the film by the positively poled field. One possible mechanism is that the contribution from the photoexcited holes is enhanced by injected holes under illumination and the negative polarization charge becomes a barrier during the discharging process, resulting in an increased macroscopic current density. For the negatively poled area (Figure 5b), the SP increased significantly following illumination with average charging lifetimes of ∼93.7 s for the initial illumination stage and ∼75.8 s for the second illumination stage. The sharp increase in SP could be attributed to the recombination of photoinduced holes with the injected negative charges on the surface of BFO, and further compensation of the SP by the positive polarization charges. When the light is switched off, the SP decays exponentially with average lifetimes of ∼236.2 and ∼104.3 s for the first and second dark stages, respectively. The longer observed lifetime for the discharging that accompanies the light-to-dark transition can be ascribed to the photoinduced holes depleted with the injected electrons from the tip where positive polarization charge plays the same role—that of a barrier for the relaxation of the SP. Under the negatively poled condition the photoinduced electrons move to the bottom electrode and induce a transit current. We remark on the additional domain wall contribution to the ferroelectric photovoltaic effect that is due to nanoscale steps of the electrostatic potential occurring at the ferroelectric domain walls in BFO.[2,22] Such electrostatic potential offset causes a band bending across the domain wall,[4] similar to the band bending in the depletion layer of a *p*−*n* junction. Here the variations in the local SP were mapped as functions of illumination intensity and applied voltage, including switching. We applied a series of dc biases ranging from −10 to +10 V with a step of 2 V using line poling,[23] and subsequent collection of PFM and KPFM images over an area of 10 × 10 μm^2 (Figure 6a and 6b, respectively). A poled area with a step of 8 × 0.72 μm^2 was observed through the out-of-plane phase image (Figure 6a), indicating that the domain was switched with sufficiently large dc bias. Since the number of domain walls changes under different values of dc bias, this confirms that through measurement of photogenerated current and corresponding SP that the open-circuit voltage increases linearly with the number of domain walls.[2,4]

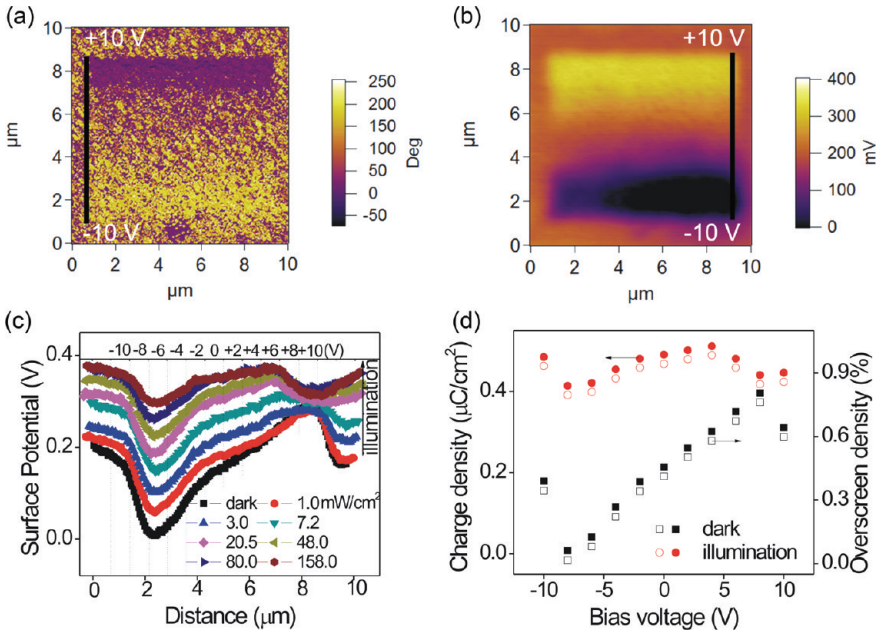

Figure 6. (*a*) PFM phase image and (*b*) KPFM surface potential distribution in the dark of the area scanned with the poled voltage biases from −10 to +10 V with a 2 V step (from bottom to top) to the tip. (c) Surface potential line profile obtained in the dark and under illumination from KPFM surface potential images. (d) Surface charge and overscreened densities calculated from the SP in the dark and under illumination at 158 mW/cm^2.

We note that the SP behavior in the dark is consistent with reported observations in heteroepitaxial $PbTiO_3$ films,[11] and that the origin of the SP under dark conditions is from both polarization and screened charges. Once the illumination is turned on and its intensity increased, the SP profile evolutions reflect the photovoltaic effect based on the variation of domain wall number (Figure 6c). The surface charge density and excess screening charge can be estimated by treating these contributions as parallel capacitances,[24] and using the measured remnant polarization of 52 μC/cm^2, and relative dielectric constant of 220 for these films (Figure 6d). With the onset of illumination, the negative contribution increases gradually, indicating that the injected electrons were recombined with the photoinduced holes. With increased negative dc bias voltage, the domain wall number is reduced and the corresponding domain wall contribution to the photocurrent should also decrease. As for the positively poled area, we observe that the SP changes are different below and above the coercive voltage (~5 V). Below the coercive voltage, the SP increases linearly for +2 and +4 V and is seen to saturate when the illumination intensity is ~158 mW/cm^2, indicating that photoinduced holes combine with the injected holes. Above the coercive voltage, the domain walls begin to move and the domain wall number gradually decreases in the poled area with higher bias voltage. As a result, the dissociation of photoinduced electron−hole pairs across the domain wall is reduced, causing the SP to begin to decrease for the area poled using +6 and +8 V. Interestingly, as the bias voltage increased from +8 to +10 V, the SP is seen to decrease at low illumination intensity (<20.5 mW/cm^2), but is seen to increase for high illumination intensity (>20.5 mW/cm^2) (This is not observable in Figure 4b where only one fixed voltage was applied.) Under low illumination intensity, the SP decreased because of reduced overscreening charge density.[11] However, when the illumination intensity is increased (>20.5 mW/cm^2), the photoinduced holes compensate the overscreened charges and dominate the SP, as seen by a modest increase for the area poled at +10 V.

Finally we remark that molecular adsorbates are known to contribute to the surface potential and specifically to the ferroelectric stability in ultrathin films and nanostructures;[25] in fact, the slow loss of electrostatic force microscopy contrast following poling for bulk-like $BaTiO_3$ takes place on the time scale of many tens of hours,[26] and not minutes as we observe presently. Nevertheless rigorous experimental and theoretical studies are needed to understand the contribution from adsorbates in the presence of a local field in ambient conditions to the time evolution of the SP contrast.

CONCLUSIONS

In summary, we demonstrate the value of combining KPFM and PFM in mapping the evolution of SP arising from the dynamics of a photoinduced charge within a semiconducting ferroelectric film. The time-dependence to the SP is obtained for the as-grown film and is attributed to a relaxation of both free and screened charges, whereas for the poled area the time

dependence is impacted by the direction of polarization, with contributions both from the bulk ferroelectric photovoltaic effect and from number-dependent domain walls.

METHODS

Sample Preparation. High quality epitaxial BFO films (~140 nm thick) were grown on 0.5 wt % Nb-doped $SrTiO_3$ (001)-oriented (NSTO) single crystal substrates at 550 °C *via* pulsed laser deposition using a KrF excimer laser (λ = 248 nm). The partial oxygen pressure was about 50 mTorr and the energy fluence of the KrF excimer laser at the target was ~1 J/cm^2. Thickness was determined *via* measurement of a step height and validated using cross-section SEM.

Macroscopic Photovoltaic Measurements. Semitransparent Pt top electrodes (*ca.* 10−20 nm in thickness and ~100 μm in diameter) were sputter-deposited on the BFO films for macroscopic photovoltaic and ferroelectric testing. The macroscopic photovoltage and photocurrent measurements were collected using an electrometer (Keithley 6487) under illumination through the top electrodes.

Kelvin Probe and Piezoresponse Force Microscopy. KPFM and PFM images were recorded (Asylum Research MFP-3D) using a Pt-coated cantilever (Olympus AC240, nominal spring constant ~2 N/m, resonant frequency ~70 kHz) with the NSTO substrate held electrically to ground. All of the data shown were obtained using the identical AFM cantilever. To produce the photogenerated charge, samples were illuminated using a 150 W tungsten halogen lamp. To determine the local ferroelectric contribution to the photovoltaic effect, a voltage was applied to the tip during the first scan using a contact mode to switch the polarization of BFO film. The SP signal was recorded in successive scans, first in the dark and again immediately under steady-state illumination. To eliminate the pyroelectric contribution to the measured potential, data were collected using relatively slow scanning rates (0.3−0.5 Hz) and analyzed from within a region of uniform illumination intensity by avoiding a strong focus.[3] For the KPFM and PFM data shown in Figure 1, the scan rate for poling was 1.0 Hz; however, all other data shown in the manuscript was collected following the use of the slower scanning rate for poling (0.3 Hz).

Conflict of Interest: The authors declare no competing financial interest.

Acknowledgment. Work at Drexel was supported by the ARO under W911NF-08-1-0067. G.C. was supported by the NSF under DMR 0907381.

Supporting Information Available: X-ray diffraction characterization of the film; macroscopic ferroelectric hysteresis loops, leakage currents and the local ferroelectric properties; PFM response collected using a slower scan rate for poling as described in the Methods section; additional KPFM experimental results. This material is available free of charge *via* the Internet at http://pubs.acs.org.

REFERENCES AND NOTES

1. Choi, T.; Lee, S.; Choi, Y. J.; Kiryukhin, V.; Cheong, S. W. Switchable Ferroelectric Diode and Photovoltaic Effect in $BiFeO_3$. *Science* **2009**, *324*, 63–66.
2. Yang, S. Y.; Seidel, J.; Byrnes, S. J.; Shafer, P.; Yang, C. H.; Rossell, M. D.; Yu, P.; Chu, Y. H.; Scott, J. F.; Ager, J. W., III; *et al*. Above-bandgap Voltages from Ferroelectric Photovoltaic Devices. *Nat. Nanotechnol.* **2010**, *5*, 143–147.
3. Alexe, M.; Hesse, D. Tip-Enhanced Photovoltaic Effects in Bismuth Ferrite. *Nat. Commun.* **2011**, *2*, Art. No. 256.
4. Huang, H. Solar Energy Ferroelectric Photovoltaics. *Nat. Photonics* **2010**, *4*, 134–135.
5. Ji, W.; Yao, K.; Liang, Y. C. Bulk Photovoltaic Effect at Visible Wavelength in Epitaxial Ferroelectric $BiFeO_3$ Thin Films. *Adv. Mater.* **2010**, *22*, 1763.
6. Shao, R.; Nikiforov, M.; Bonnell, D. A. Photoinduced Charge Dynamics on $BaTiO_3$ Surface Characterized by Scanning Probe Microscopy. *Appl. Phys. Lett.* **2006**, *89*, 112904.
7. Ihlefeld, J. F.; Podraza, N. J.; Liu, Z. K.; Rai, R. C.; Xu, X.; Heeg, T.; Chen, Y. B.; Li, J.; Collins, R. W.; Musfeldt, J. L.; *et al*. Optical Band Gap of $BiFeO_3$ Grown by Molecular-Beam Epitaxy. *Appl. Phys. Lett.* **2008**, *92*, 142908.
8. Spadafora, E. J.; Demadrille, R.; Ratier, B.; Grevin, B. Imaging the Carrier Photogeneration in Nanoscale Phase Segregated Organic Heterojunctions by Kelvin Probe Force Microscopy. *Nano Lett.* **2010**, *10*, 3337–3342.
9. Liscio, A.; Palermo, V.; Samori, P. Nanoscale Quantitative Measurement of the Potential of Charged Nanostructures by Electrostatic and Kelvin Probe Force Microscopy: Unraveling Electronic Processes in Complex Materials. *Acc. Chem. Res.* **2010**, *43*, 541–550.
10. Sinensky, A. K.; Belcher, A. M. Label-free and High-Resolution Protein/DNA Nanoarray Analysis Using Kelvin Probe Force Microscopy. *Nat. Nanotechnol.* **2007**, *2*, 653–659.
11. Kim, Y.; Bae, C.; Ryu, K.; Ko, H.; Kim, Y. K.; Hong, S.; Shin, H. Origin of Surface Potential Change During Ferroelectric Switching in Epitaxial $PbTiO_3$ Thin Films Studied by Scanning Force Microscopy. *Appl. Phys. Lett.* **2009**, *94*, 032907.
12. Kalinin, S.; Bonnell, D. Screening Phenomena on Oxide Surfaces and Its Implications for Local Electrostatic and Transport Measurements. *Nano Lett.* **2004**, *4*, 555–560.
13. Liscio, A.; Palermo, V.; Gentilini, D.; Nolde, F.; Mullen, K.; Samori, P. Quantitative Measurement of the Local Surface Potential of π-Conjugated Nanostructures: A Kelvin Probe Force Microscopy Study. *Adv. Funct. Mater.* **2006**, *16*, 1407–1416.
14. Qu, T. L.; Zhao, Y. G.; Xie, D.; Shi, J. P.; Chen, Q. P.; Ren, T. L. Resistance Switching and White-Light Photovoltaic Effects in $BiFeO_3$/Nb-$SrTiO_3$ Heterojunctions. *Appl. Phys. Lett.* **2011**, *98*, 173507.
15. Yang, H.; Luo, H. M.; Wang, H.; Usov, I. O.; Suvorova, N. A.; Jain, M.; Feldmann, D. M.; Dowden, P. C.; DePaula, R. F.; Jia, Q. X. Rectifying Current-Voltage Characteristics of $BiFeO_3$/Nb-Doped $SrTiO_3$ Heterojunction. *Appl. Phys. Lett.* **2008**, *92*, 102113.
16. Watanabe, Y. Tunneling Current Through a Possible All-Perovskite Oxide *p*−*n* Junction. *Phys. Rev. B* **1998**, *57*, R5563–R5566.
17. Tanaka, H.; Zhang, J.; Kawai, T. Giant Electric Field Modulation of Double Exchange Ferromagnetism at Room Temperature in the Perovskite Manganite/Titanate *p*−*n* Junction. *Phys. Rev. Lett.* **2001**, *88*, 027204.
18. Schultz, A. M.; Zhang, Y.; Salvador, P. A.; Rohrer, G. S. Effect of Crystal and Domain Orientation on the Visible-Light Photochemical Reduction of Ag on $BiFeO_3$. *ACS Appl. Mater. Interfaces* **2011**, *3*, 1562–1567.
19. Wu, W.; Guest, J. R.; Horibe, Y.; Park, S.; Choi, T.; Cheong, S. W.; Bode, M. Polarization modulated Rectification at Ferroelectric Surfaces. *Phys. Rev. Lett.* **2010**, *104*, 217601.
20. Unold, T.; Schock, H. Nonconventional (Non-silicon-Based) Photovoltaic Materials. *Annu. Rev. Mater. Res.* **2011**, *41*, 297–321.
21. Clark, S. J.; Robertson, J. Energy Levels of Oxygen Vacancies in $BiFeO_3$ by Screened Exchange. *Appl. Phys. Lett.* **2009**, *94*, 022902.
22. Seidel, J.; F, D.; Yang, S.-Y.; Alarcon-Llado, E.; Wu, J.; Ramesh, R.; Ager, J. W. Efficient Photovoltaic Current Generation at Ferroelectric Domain Walls. *Phys. Rev. Lett.* **2011**, *107*, 126805.
23. Wong, M. F.; Herng, T. S.; Zhang, Z.; Zeng, K.; Ding, J. Stable Bipolar Surface Potential Behavior of Copper-Doped Zinc

Oxide Films Studied by Kelvin Probe Force Microscopy. *Appl. Phys. Lett.* **2010**, *97*, 232103.
24. Chen, X.; Yamada, H.; Horiuchi, T.; Matsushige, K.; Watanabe, S.; Kawai, M.; Weiss, P. Surface Potential of Ferroelectric Thin Films Investigated by Scanning Probe Microscopy. *J. Vac. Sci. Technol., B* **1999**, *17*, 1930–1934.
25. Spanier, J.; Kolpak, A.; Grinberg, I.; Urban, J. J.; Ouyang, L.; Yun, W.-S.; Rappe, A. M.; Park, H. Ferroelectric Phase Transition in Individual $BaTiO_3$ Nanowires. *Nano Lett.* **2006**, *6*, 735–739.
26. Nonnenmann, S.; Spanier, J. E. Ferroelectricity in Chemical Nanostructures: Proximal Probe Characterization and the Surface Chemical Environment. *J. Mater. Sci.* **2009**, *44*, 5205.